8th International Conference on Sandwich Structures
ICSS 8
A. J. M. Ferreira (Editor)

DAMAGE TOLERANCE OF A SANDWICH PANEL WITH A CRACKED SQUARE HONEYCOMB CORE LOADED IN SHEAR

I. Quintana Alonso and N.A. Fleck

Cambridge University Engineering Department, Trumpington Street, Cambridge, CB2 1PZ, UK
e-mail: iq201@cam.ac.uk; naf1@cam.ac.uk

Keywords: finite element analysis, fracture toughness, elastic behaviour, honeycomb

Summary. *We explore the shear fracture strength of a sandwich panel made from an elastic brittle diamond-celled honeycomb, containing a centre-crack. The honeycomb fails when the local stress attains the tensile or compressive strength of the solid, or by local buckling. Finite element predictions are given for the unnotched strength, and for the fracture toughness. These predictions, together with conventional linear elastic fracture mechanics, are used to construct a failure map with axes given by the geometry of the cracked sandwich panel. The strength of the sandwich structure is calculated according to the dominant failure mechanisms, which depend upon the tensile failure strain of the solid and upon the relative density of the honeycomb. The relevance of the failure map is illustrated through material-property charts. An extension of the method to cyclic loading is discussed.*

1 INTRODUCTION

Honeycomb materials are often used in applications where severe mechanical loads and operating conditions lead to damage. Examples include catalytic converters for automobiles, filters for liquid metal, absorbers for solar receivers, supports for space mirrors, and orthopaedic implants for bone repair. Cracks can exist in the honeycomb and cause a significant decrease of its fracture strength. Commonly, the honeycomb core is loaded in a sandwich panel configuration with stiff and strong face-sheets. The damage tolerance of these sandwich structures is of concern and motivates the present study.

In this paper we explore the *shear* fracture strength of a sandwich panel made from an elastic brittle diamond-celled honeycomb. The core contains a central crack, and loading is parallel to the faces of the sandwich panel, see Fig. 1a. Finite element simulations and simple analytical models are used to determine the strength of the sandwich structure.

A recent numerical study of the *tensile* fracture strength of a cracked sandwich panel [1], revealed that linear elastic fracture mechanics applies when a K-field exists on a scale larger than the cell size. But there is also a regime of geometries for which no K-field exists. In this regime the stress concentration at the crack tip is negligible and the net strength of the cracked specimen is comparable to the unnotched strength. We anticipate similar behaviour for a sandwich panel subjected to remote shear.

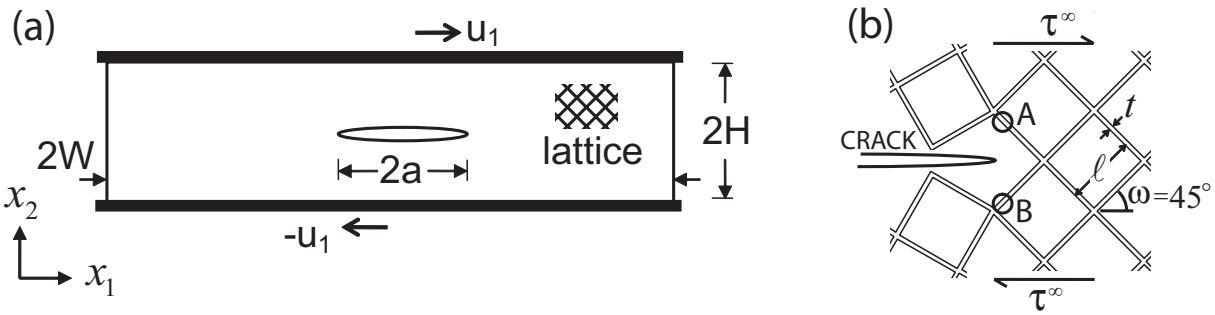

Fig. 1 (a) Sandwich panel containing a cracked diamond-celled honeycomb core subjected to shear loading. (b) Sketch of the diamond-celled topology.

Quintana-Alonso and Fleck [1] assumed that local failure occurs when the maximum tensile stress at any point in the lattice attains the tensile fracture strength of the solid. In contrast, a sandwich panel subjected to remote shear may fail by (i) local buckling of the cell walls, (ii) local compressive failure or (iii) local tensile failure of the cell walls. We examine all three possibilities in the current study.

1.1 Description of the problem

Consider the sandwich geometry shown in Fig. 1a. The panel is of width $2W$, height $2H$, and contains a centre-crack of length $2a$. Shear displacements are applied to the top and bottom nodes of the core in order to simulate the relative motion of the face-sheets.

The geometry of the diamond-celled lattice, sketched in Fig. 1b, is described by its cell size ℓ and wall thickness t. A fixed core angle of $\omega = 45^\circ$ is assumed. The relative density of the core $\bar{\rho}$, defined as the density of the honeycomb divided by that of the solid from which it is made, scales with stockiness $\bar{t} = t/l$ as

$$\bar{\rho} = \bar{t}\left(2 - \bar{t}\right) \qquad (1)$$

The solid material is linear elastic to fracture. It has a Young's modulus E_s, a tensile fracture strength σ_t, and a compressive fracture strength σ_c.

The normalised gross fracture stress τ^∞/σ_t is a function of the geometric non-dimensional groups t/ℓ, a/ℓ, H/ℓ, and H/W; and of the material groups σ_t/E_s and σ_t/σ_c. We shall explore the effect of these parameters upon the shear fracture strength, τ^∞/σ_t, but limit attention to the practical case where H/W is small.

1.2 Scope of the study

First, the unnotched strength of the sandwich panel with a honeycomb core is determined. Second, the mode II fracture toughness of the lattice is calculated. These predictions are used

to construct a fracture map for the centre-cracked panel, with non-dimensional axes given in terms of the sandwich geometry. The relevance of the fracture map to engineering materials is illustrated through material-property charts. Finally, the study is extended to the fatigue strength of lattices.

2 UNNOTCHED STRENGTH OF THE SANDWICH PANEL

2.1 Local Tensile or Compressive Failure of the Cell Walls

Consider a sandwich panel subjected to a shearing displacement of $\pm u_1$ on its faces, as shown in Fig. 1a. In the absence of a crack, the stress state within the honeycomb can be determined by classical beam theory. The cell walls in the $+45^\circ$ direction are loaded in tension, while those in the -45° direction are in compression.

Straightforward analysis reveals that the unnotched shear strength τ_u^T for *tensile local failure* scales with the tensile fracture strength of the solid σ_t and with $\overline{t}$ according to

$$\tau_u^T = \frac{\overline{t}}{1+3\overline{t}/2}\sigma_t \tag{2}$$

This expression takes into account both stretching and bending of the cell walls. It is acceptable to neglect the bending contribution at low relative densities ($\overline{t} < 0.1$), and Eq. (2) then reduces to

$$\tau_u^T = \overline{t}\,\sigma_t \tag{3}$$

The unnotched shear strength for *compressive local failure* τ_u^C takes the same functional form as Eq. (3), but now scales with σ_c, as given in Table 1. It is evident that the local dominant failure mechanism depends upon the ratio of tensile to compressive fracture strength of the solid material σ_t/σ_c.

LOCAL FAILURE	UNNOTCHED STRENGTH	FRACTURE TOUGHNESS
Tensile	$\tau_u^T = \overline{t}\,\sigma_t$	$K_{IIC}^T = 0.44\overline{t}\,\sigma_t\sqrt{\ell}$
Compressive	$\tau_u^C = \overline{t}\,\sigma_c$	$K_{IIC}^C = 0.44\overline{t}\,\sigma_c\sqrt{\ell}$
Buckling	$\tau_u^B = 1.88\overline{t}^3 E_s$	$K_{IIC}^B = 2.75\overline{t}^3 E_s\sqrt{\ell}$

Table. 1. Unnotched strength of the sandwich panel and fracture toughness of the lattice.

2.2 Cell Wall Buckling

The honeycomb may also fail by elastic buckling of its cell walls. Finite element simulations indicate that buckling occurs in a periodic cruciform manner, see Fig. 2. Each cell wall behaves as an Euler strut of length ℓ, but with end rotational restraint provided by the adjoining tensile bars. The buckling load is [2]

$$P_{\text{crit}} = \frac{n^2 \pi^2 E_s I}{\ell^2} \tag{4}$$

with $I = t^3/12$ per unit depth. The factor n describes the rotational stiffness of the joints where the cell walls meet. If rotation is freely allowed, $n = 0.5$; if no rotation is possible, $n = 2$. The unnotched shear strength for local buckling follows from equilibrium, giving

$$\tau_u^B = n^2 \frac{\pi^2}{12} \bar{t}^3 E_s \tag{5}$$

Finite element calculations suggest $n = 1.51$. A simple direct estimate for n can be obtained. In the buckled state, the tensile bars inclined at $+45^\circ$ are subjected to alternating point torques of $\pm T$, from one joint to the next (Fig. 2). The joints also rotate by $\pm\phi$, and simple beam theory for the tensile bars provides the desired torsional stiffness $T/\phi = 4E_s I/\ell$. Newmark [3] gives a useful approximate formula for the dependence of n in Eq. (5) upon the value of T/ϕ; his formula implies $n = 1.44$, which is in satisfactory agreement with the FE result of $n = 1.51$.

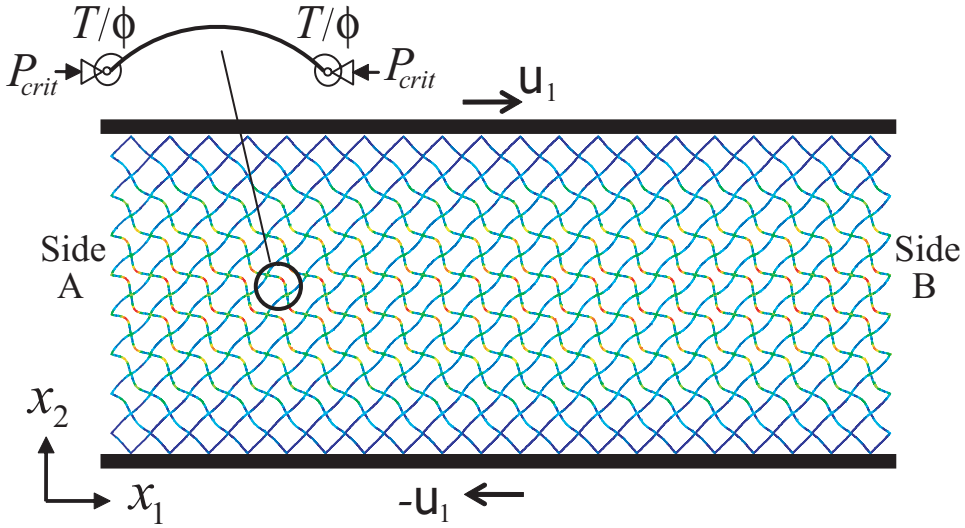

Fig. 2. Buckling of an unnotched panel subjected to remote shear. The face-sheets are allowed to displace in the x_2-direction, but rotation is not permitted. The boundary conditions on the sides of the specimen are: $u_1^A = u_1^B$; $u_2^A = u_2^B$; $\theta^A = \theta^B$.

3 PREDICTION OF FRACTURE TOUGHNESS

The fracture toughness of the diamond-celled honeycomb is obtained by considering a cracked lattice, with an outer K-field, following Romijn and Fleck [4]. The displacement field $\boldsymbol{u}$ associated to a K-field is applied to the outer boundary of this lattice, as given by Sih et al. [5], see Fig. 3.

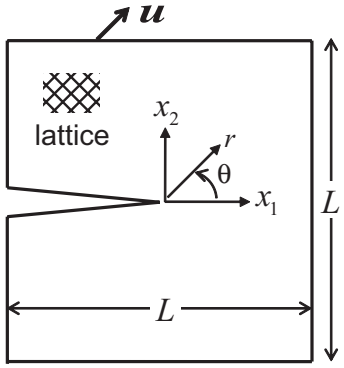

Fig. 3. Finite element model used in the fracture toughness predictions.

Linear elastic calculations were performed using the commercial finite element code Abaqus (version 6.7-1). The lattice was meshed with Timoshenko beam elements (type *B21* in Abaqus notation). A mesh convergence study suggested that a mesh of side $L = 600\ell$ is adequate.

The mode II fracture toughness for *tensile local failure* K_{IIC}^{T} is calculated by equating the maximum tensile stress at any point in the mesh to the tensile strength σ_t of the solid. A series of FE simulations have been performed with $\overline{t}$ in the range 10^{-3} to 10^{-1}. The results show that K_{IIC}^{T} scales linearly with $\overline{t}$ and is represented by the regression

$$K_{IIC}^{T} = 0.44\sigma_t \overline{t}\sqrt{\ell} \tag{6}$$

to within a few percent.

Alternatively, the fracture toughness for *compressive local failure* K_{IIC}^{C} is calculated by equating the minimum compressive stress at any point in the mesh to the compressive strength σ_c of the solid. Eq. (6) again applies, but with $\left(K_{IIC}^{T}, \sigma_t\right)$ replaced by $\left(K_{IIC}^{C}, \sigma_c\right)$, as listed in Table 1. The failure site within the honeycomb is shown in Fig. 1b: it is labelled A for tensile failure, and B for compressive.

Local buckling can also occur at the crack tip. An eigenvalue extraction is used in the FE calculations to determine the bifurcation load for buckling, giving a mode II fracture toughness of

$$K_{IIC}^{B} = 2.75E_s \overline{t}^{3}\sqrt{\ell} \tag{7}$$

Selected nonlinear elastic simulations with small initial imperfections confirm the validity of Eq. (7). In the post-buckling regime, the levels of tensile and compressive strain are significantly elevated near the crack tip, and it is concluded that K_{IIC}^{B} serves as a useful fracture parameter.

Figure 4 shows the deformed mesh near the crack tip for (a) the fundamental equilibrium path, and for (b) the first eigenmode. The fundamental solution is characterised by bending of the cell walls. Narrow zones of high bending stress emanate from the crack tip along the $\pm 45^{\circ}$ radial directions. The length of these zones scales inversely with $\overline{t}$, as discussed by Fleck and Qiu [6]. The first eigenmode involves buckling of the crack tip struts.

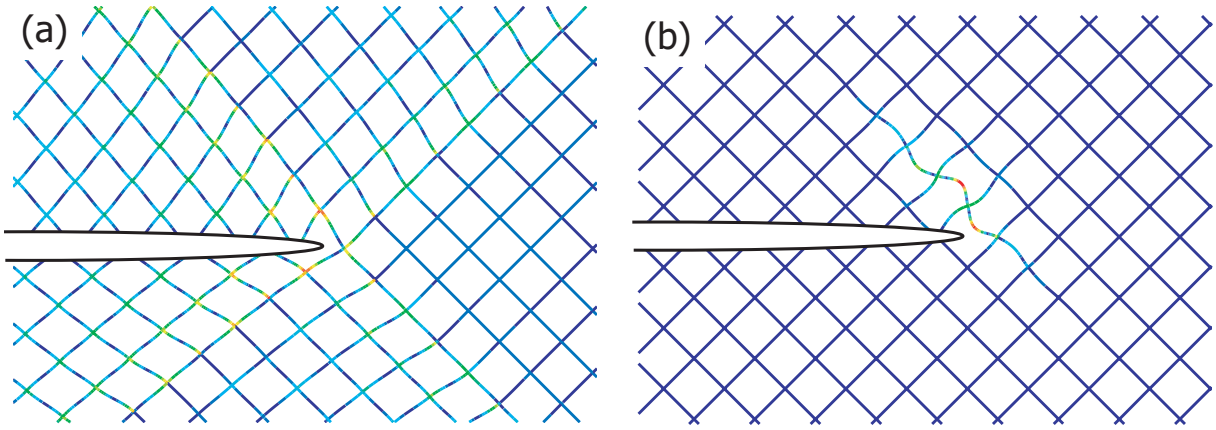

Fig. 4. Deformed mesh near the crack tip of a lattice subjected to a remote K-field on its outer boundary. (a) Fundamental equilibrium solution. (b) First eigenmode.

4 FAILURE MAPS FOR THE CRACKED SANDWICH PANEL

The above results are summarised in Table 1. They can be used to construct a fracture map, with suitably chosen non-dimensional axes. The mode II fracture toughness K_{IIC} of the diamond-celled lattice is taken as $\min\left(K_{IIC}^{C}, K_{IIC}^{T}, K_{IIC}^{B}\right)$. It depends upon the lattice geometry and the material properties of the solid from which it is made. Likewise, the unnotched shear strength τ_u of the sandwich panel is $\min\left(\tau_u^{C}, \tau_u^{T}, \tau_u^{B}\right)$.

We limit attention to materials which satisfy $\sigma_c/\sigma_t > 1$, so that compressive local failure of the unnotched lattice and of the cracked lattice never occur. This is not a severe restriction on material choice: almost all engineering solids have the characteristic $\sigma_c/\sigma_t > 1$.

Note from Table 1 that the unnotched strength is buckling-governed when $\tau_u^{B}/\tau_u^{T} \equiv 1.88\,\overline{t}^{\,2}E_s/\sigma_t < 1$. Similarly, the fracture toughness is buckling-governed when $K_{IIC}^{B}/K_{IIC}^{T} \equiv 6.25\,\overline{t}^{\,2}E_s/\sigma_t < 1$. Thus, the value of the non-dimensional group $\Sigma \equiv \sigma_t/\overline{t}^{\,2}E_s$ dictates whether the unnotched strength and the fracture toughness are due to buckling or tensile local failure. This competition of local failure criteria is summarised in Table 2.

	UNNOTCHED STRENGTH		FRACTURE TOUGHNESS	
$\Sigma \equiv \frac{\sigma_t}{E_s \bar{t}^2}$	Buckling?	Tensile Failure?	Buckling?	Tensile Failure?
< 1.88	—	✓	—	✓
$1.88 - 6.25$	✓	—	—	✓
> 6.25	✓	—	✓	—

Table 2. The unnotched strength and fracture toughness are controlled by local cell wall buckling or by local tensile failure. The weakest mode of local failure is dictated by the value of Σ.

Now consider the fracture strength of the sandwich panel containing a finite centre-crack of length $2a$, for any given value of Σ. It is instructive to construct a failure map for the cracked sandwich panel using axes $\left(\ell/a, \ell/H\bar{t}\right)$, as shown in Fig. 5.

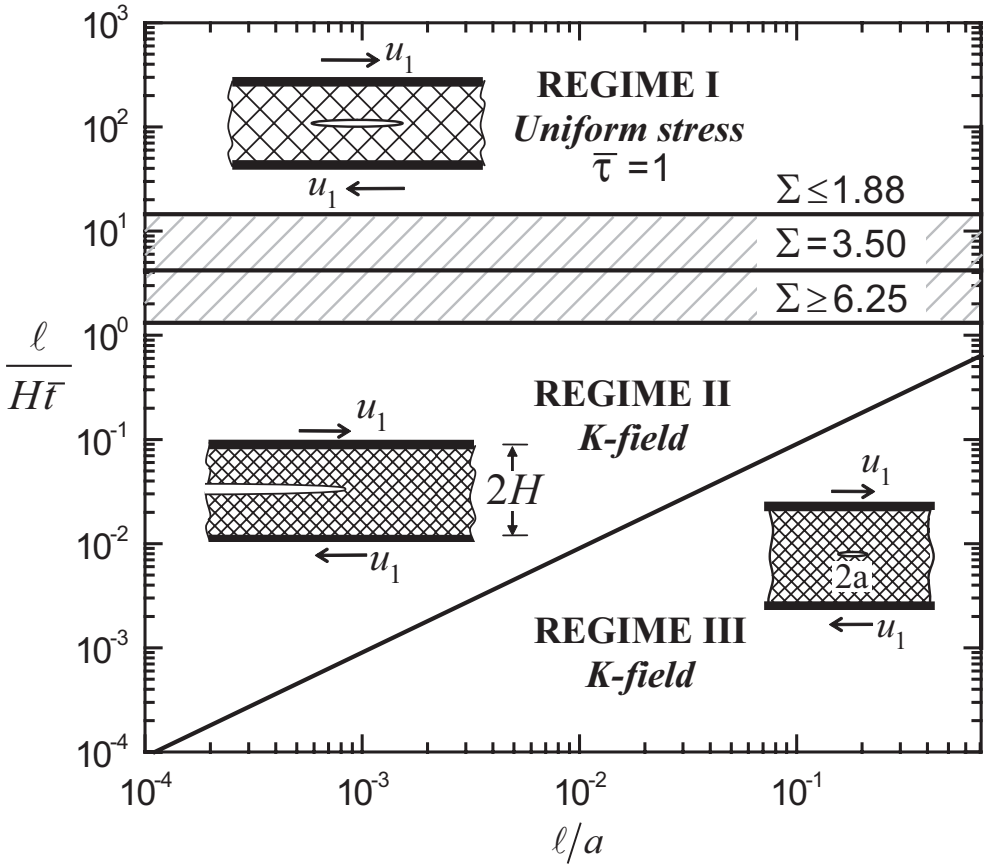

Fig. 5. Fracture map for a panel containing a centre crack and subjected to prescribed shear displacements. The map is valid for small H/W.

Three distinct regimes of the map can be identified. In Regime I, no stress concentration exists and the net-section strength equals the unnotched strength. In Regimes II and III, LEFM applies and the net-section strength is dictated by the fracture toughness. Regime II relates to cracks which are much longer than the height of the panel $2H$, while Regime III exists for short cracks. The details are as follows.

Define the non-dimensional net-section strength as

$$\overline{\tau} \equiv \frac{\tau^{\infty}}{\left(1-a/W\right)\tau_u^T} \quad , \quad \Sigma \le 1.88 \tag{8}$$

and

$$\overline{\tau} \equiv \frac{\tau^{\infty}}{\left(1-a/W\right)\tau_u^B} \quad , \quad \Sigma > 1.88 \tag{9}$$

consistent with Table 2. In order to construct the map we consider the value of $\overline{\tau}$ for each regime in turn.

Regime I: No stress concentration exists at the crack tip. The stress state within the lattice is such that the bending component is negligible with respect to the stretching contribution. It is a damage tolerant regime: the net strength of the panel equals the unnotched strength, and $\overline{\tau} = 1$.

Regime II: The crack is sufficiently long compared to the height of the sandwich panel that the core behaves as an orthotropic elastic strip with a semi-infinite crack. The stress intensity factor for this geometry is given by

$$K_{II} = F_{II}\tau^{\infty}\sqrt{H} \tag{10}$$

where the calibration function is $F_{II} = 2^{3/4}\sqrt{\overline{t}}\left(1-a/W\right)^{-1}$, see reference [1]. Failure occurs when the stress intensity factor, K_{II}, reaches the critical value, K_{IIC}. Consequently, we have

$$\begin{aligned} \overline{\tau} &= 0.141\left(\ell/H\overline{t}\right)^{1/2} \quad , \quad \Sigma \le 1.88 \\ \overline{\tau} &= 0.140\Sigma\left(\ell/H\overline{t}\right)^{1/2} \quad , \quad 1.88 < \Sigma < 6.25 \\ \overline{\tau} &= 0.872\left(\ell/H\overline{t}\right)^{1/2} \quad , \quad \Sigma \ge 6.25 \end{aligned} \tag{11}$$

Regime III: The crack is much smaller than the height and width of the sandwich panel. The K-calibration for an orthotropic panel containing a short central crack of length $2a$ is approximately

$$K_{II} = \frac{\tau^{\infty}\sqrt{\pi a}}{\left(1-a/W\right)} \tag{12}$$

as reported in [1]. Upon equating K_{II} to K_{IIC} we obtain

$$\begin{aligned} \bar{\tau} &= 0.248\left(\ell/a\right)^{1/2} \quad , \quad \Sigma \le 1.88 \\ \bar{\tau} &= 0.132\Sigma\left(\ell/a\right)^{1/2} \quad , \quad 1.88 < \Sigma < 6.25 \\ \bar{\tau} &= 0.872\left(\ell/a\right)^{1/2} \quad , \quad \Sigma \ge 6.25 \end{aligned} \tag{13}$$

The boundaries of the map follow immediately from equating $\bar{\tau}$ in neighbouring regimes. Boundary between Regimes I / II:

$$\begin{aligned} \ell/H\bar{t} &= 14.61 \quad , \quad \Sigma \le 1.88 \\ \ell/H\bar{t} &= 51.38/\Sigma^2 \quad , \quad 1.88 < \Sigma < 6.25 \\ \ell/H\bar{t} &= 1.32 \quad , \quad \Sigma \ge 6.25 \end{aligned} \tag{14}$$

Boundary between Regimes II / III:

$$\ell/\bar{t}H = 0.90\left(\ell/a\right) \quad , \quad \text{for all } \Sigma \tag{15}$$

A physical constraint on the minimum crack length is also imposed on the map: the minimum crack length in the lattice is $a/\ell = \sqrt{2}$. The resulting universal fracture map is shown in Fig. 5. Contours of $\bar{\tau}$ could be added, but their precise value is dependent on the choice of Σ.

We emphasise that $\bar{\tau} = 1$ in Regime I, while in Regime II the values of $\bar{\tau}$ are given by Eq. (11), and in Regime III by Eq. (13). A similar map has been constructed for tensile loading of the cracked sandwich panel [1]. Again, three regimes exist, and the failure map has been validated by extensive FE simulations of specific cracked geometries. Studies were undertaken over a wide range of $\left(\bar{t}, \ell/a\right)$. Good agreement between analytical formulae and numerical predictions has been noted for all regimes of behaviour, with a marked transition between regimes. These results give confidence in the fracture map presented here for remote shear loading.

4.1 Application to Engineering Materials

Recall that the competition between cell wall buckling and local tensile failure is dictated by the value of Σ, as summarised in Table 2. Σ scales with the material index σ_t/E_s and with $1/\bar{t}^2$. Thus, the value of Σ is dependent upon material choice, for any given $\bar{t}$.

A chart of the tensile strength σ_t plotted against the Young's modulus E_s has been generated for engineering materials using the commercial package CES [7], see Fig. 6. We limit materials to those which are elastic-brittle, with zero tensile ductility $\varepsilon_f = 0$. Data for a given class of materials (e.g. technical ceramics) are enclosed in property-envelopes.

Lines of constant Σ have been added to Fig. 6 for $\bar{t} = 0.01$ and 0.1. For stocky lattices with $\bar{t} = 0.1$, almost all materials possess a value of Σ which is much less than 1.88; consequently, the unnotched strength and the fracture toughness are governed by local tensile

failure. In contrast, for the more slender lattice, $\bar{t} = 0.01$, the lines $\Sigma = 1.88$ and 6.25 cut through much of the data. Therefore, there is a close competition between buckling and local tensile failure of the cell walls, and the active failure mechanism is material dependent.

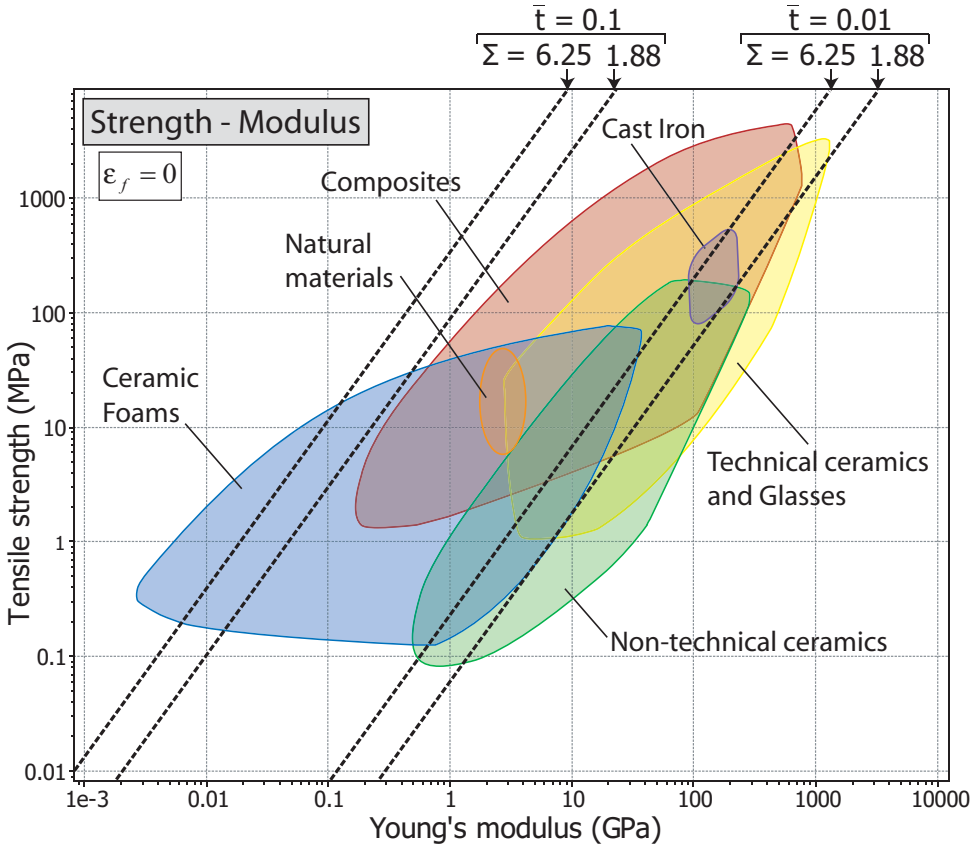

Fig. 6. Tensile strength versus Young's modulus. Materials with no tensile ductility, $\varepsilon_f = 0$.

The fracture map presented in this study (Fig. 5) also describes the *fatigue strength* of lattice materials, with the following slight modification. Replace the tensile strength σ_t by the amplitude of fatigue loading σ_e of the solid at the endurance limit (10^7 cycles). Also, replace τ^∞ by the amplitude of fatigue loading τ_a at the endurance limit for the cracked sandwich panel. Then, the unnotched fatigue strength of the lattice is given by Eq. (2), and the mode II fatigue threshold is given by

$$\left(\Delta K_{II}\right)_{th} = 0.88\sigma_e \bar{t}\sqrt{\ell} \qquad (16)$$

via Eq. (6). Buckling remains a possibility under cyclic loading and Eqs. (5) and (7) still hold. The expressions (8)-(15) apply, but with the substitution $\left(\sigma_t, \tau^\infty\right) \to \left(\sigma_e, \tau_a\right)$ for cyclic loading.

It is straightforward to also generate a fatigue chart of engineering materials using CES, with the endurance limit σ_e as the y-axis and the Young's modulus E_s as the x-axis (Fig. 7). Lines of $\Sigma = 1.88$ and 6.25 are again included in Fig. 7 for $\bar{t} = 0.01$ and 0.1.

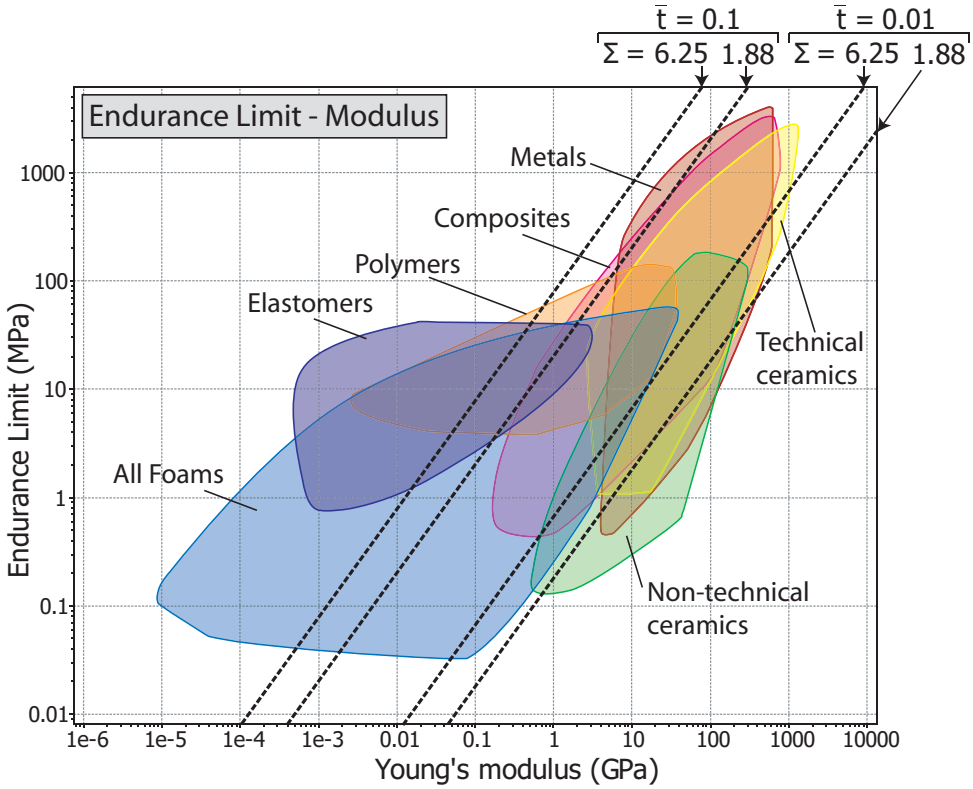

Fig. 7. Endurance limit versus Young's modulus. Note that $\Sigma \equiv \sigma_t / E_s \bar{t}^2$.

The ratio of endurance strength to tensile strength, σ_e / σ_t, is termed the fatigue ratio. It is of the order of $0.35 - 0.5$ for metallic alloys, and of the order of unity for ceramics. We note that the value of Σ is reduced by the fatigue ratio under cyclic loading.

We have included all engineering materials in the fatigue property chart of Fig. 7 in view of the fact that the cyclic stress state is given by the elastic solution at the endurance limit. Thus, in the fatigue case, our elastic-brittle analysis is not restricted to solids of low ductility. It is clear from Fig. 7 that materials exist which undergo cell wall buckling at the endurance limit for both small $\bar{t} = 0.01$ and large $\bar{t} = 0.1$. These materials include elastomers, polymers and foams. Most metallic alloys undergo fatigue failure at the cell-wall level for $\bar{t} = 0.1$, but buckle at $\bar{t} = 0.01$.

5 CONCLUDING REMARKS

We have investigated the damage tolerance of a sandwich panel containing a centrally cracked diamond-celled honeycomb core. Expressions for unnotched shear strength and mode II fracture toughness are obtained by finite element calculations. A fracture map has been constructed with axes given by the sandwich geometry. It is a useful guide for calculating the strength of the damaged sandwich structure. The dominant local failure mechanism depends upon the tensile failure strain σ_t/E_s of the solid and upon the strut stockiness $\overline{t}$.

It is recognised that brittle solids exhibit a scatter of failure strength: variable flaw sizes and a random orientation within the brittle cell walls lead to variations in the tensile strength of the solid material σ_t. Statistical variations in the cell wall strength are usually quantified by assuming a Weibull distribution. The effect of specimen geometry and Weibull modulus m upon the fracture map can then be explored. It is expected that the larger the sandwich panel the more likely it is to be strength-controlled, for a given cell size of the honeycomb. Also, the domains of toughness-controlled fracture will shrink as the Weibull modulus is decreased. This is not explored further here, but is discussed for the tensile loading of a cracked sandwich panel in [1].

Microstructural imperfections such as wavy struts and displaced joints are expected to have a knock-down effect upon the fracture properties of elastic-brittle honeycombs. The sensitivity of fracture toughness to imperfections in the form of displaced joints has been explored by Romijn and Fleck [4]. Their analysis indicates that the fracture toughness of the diamond-celled topology is imperfection-sensitive. Their results can be used to modify the strength predictions of the cracked sandwich panel with imperfections present at the cell wall level.

REFERENCES

[1] I. Quintana Alonso and N.A. Fleck, “The Damage Tolerance of a Sandwich Panel Containing a Cracked Honeycomb Core,” *J. Appl. Mech.* In print.

[2] S.P. Timoshenko and J.M. Gere, *Theory of Elastic Stability*, 2nd ed. McGraw-Hill, New York (1961).

[3] N.M. Newmark, “A Simple Approximate Formula for Effective End-Fixity of Columns,” *J. Aero. Sci.*, 16, 116 (1949).

[4] N.E.R. Romijn and N.A. Fleck, “The Fracture Toughness of Planar Lattices: Imperfection Sensitivity,” *J. Mech. Phys. Solids*, 55(12), 2538-2564 (2007).

[5] G.C. Sih, P.C. Paris and G.R. Irwin, “On Cracks in Rectilinearly Anisotropic Bodies,” *Int. J. Fract. Mech.* 1(3), 189-203 (1965).

[6] N.A. Fleck and X. Qiu, “The Damage Tolerance of Elastic-Brittle, Two-Dimensional Isotropic Lattices,” *J. Mech. Phys. Solids*, 55(3), 562-588 (2007).

[7] CES EduPack 2007, The Cambridge Engineering Selector, Granta Design, Rustat House, 62 Clifton Road, Cambridge CB1 7EG, UK.